archives
of thermodynamics
Vol. **39**(2018), No. 3, 63–83
DOI: 10.1515/aoter-2018-0020

Study of the influence of the lack of contact in plate fin and tube heat exchanger on heat transfer

DARIUSZ ANDRZEJEWSKI
MARCIN ŁĘCKI*
ARTUR GUTKOWSKI

Institute of Turbomachinery, Lodz University of Technology, Wólczanska 219/223, 93-005 Łódź, Poland

Abstract Plate fin-tube heat exchangers fins are bonded with tubes by means of brazing or by mechanical expansion of tubes. Various errors made in the process of expansion can result in formation of an air gap between tube and fin. A number of numerical simulations was carried out for symmetric section of plate fin-tube heat exchanger to study the influence of air gap on heat transfer in forced convection conditions. Different locations of air gap spanning 1/2 circumference of the tube were considered, relatively to air flow direction. Inlet velocities were a variable parameter in the simulations (1–5 m/s). Velocity and temperature fields for cases with air gap were compared with cases without it (ideal thermal contact). For the case of gap in the back of the tube (in recirculation zone) the lowest reduction (relatively to the case without gap) of heat transfer rate was obtained (average of 11%). The worst performance was obtained for the gap in the front (reduction relatively to full thermal contact in the average of 16%).

Keywords: Heat transfer; Heat exchanger; Computational fluid dynamics

Nomenclature

A	–	area, m^2
d	–	diameter, m
f	–	flow friction factor
g	–	gravitational acceleration, m/s^2

*Corresponding Author. Email: marcin.lecki@pl.lodz.pl

I	–	turbulence intensity
j	–	Colburn factor
k	–	kinetic energy of turbulence, m^2/s^2
L	–	length, m
p	–	pressure, Pa
P	-Ő	tube pitch, m
$\dot{Q}$	–	heat transfer rate, W
$\dot{q}$	–	heat flux, W/m^2
R_{eq}	–	equivalent fin radius, m
r	–	outer radius of the tube ($r = d_o/2$), m
T	–	temperature, K
U	–	overall thermal conductance, $W/(m^2K)$
u	–	velocity, m/s
x, y, z	–	Cartesian coordinates, m

Greek symbols

α	–	heat transfer coefficient, $W/(m^2K)$
β	–	volumetric expansion coefficient, 1/K
δ	–	thicknes, width spacing, mm
η	–	fin efficiency
θ	–	dimensionless temperature excess
λ	–	thermal conductivity, W/(mK)
μ	–	dynamic viscosity, $kgm\,s^{-1}$
ω	–	specific dissipation rate, 1/s

Subscripts

ave	–	average
f	–	fin
g	–	gap
i	–	inside, inner
in	–	inlet
l	–	longitudinal
o	–	outer, outside
t	–	tube, transverse
tot	–	total
w	–	wall

1 Introduction

Plate-fin and tube heat exchangers are the most widely used as evaporators and condensers in refrigeration systems (commercial refrigeration) and in other applications where heat transfer between liquid or evaporating/condensing fluid and gaseous working fluid is required. Proven technology, reliability and relatively low cost of manufacture make plate fin and tube heat exchangers very popular, not only as components of refrig-

eration units, but also as gas coolers/heaters, recuperative heaters, dryers etc. During their manufacture a thermal and mechanical contact between tubes and fins has to be created. The contact is usually achieved by a tube expansion (plastic deformation of the tube by moving expansion die or by applying pressure at its inner surface). These mechanical methods of expansion cause additional thermal resistance at the tube-fin interfaces, due to gaps between contact surfaces of fin collars and tubes [1]. The gaps can also be created because of the wear of the heat exchanger, e.g., in the result of corrosion. The quality of the joint can be improved by brazing the tube to the fin (soldering process is discussed in detail in [2,3]). Because of the additional amount of energy needed for soldering process and some technical difficulties (ensuring high purity of soldered surfaces) mechanical methods of expansion are the most frequently chosen.

Aside from the experimental research aimed at estimating the thermal contact resistance [4,5], its value is also obtained through semi-empirical methods, partly based on numerical analysis. Taler and Oclon [6] and Taler and Cebula [7] changed iteratively the value of contact resistance in their computational fluid dynamics (CFD) model in such a way that the thermal and flow quantities obtained from numerical solution agreed with the measured ones. Less attention has been paid to cases where there is a lack of contact with the plate-fin along a part of the tube perimeter (no contact between fin collar and tube). Recently the topic was addressed by Singh *et al.* [8] who proposed a CFD model of a finned heat exchanger with a variable contact surface area between the tube and the fin. They considered several cases of gaps of different sizes. They found that the presence of gaps influenced heat transfer and flow (pressure drop) in the significant way. In contrast to [8], where several triangular gaps are distributed evenly along joint circumference, our work presents CFD analysis of plate-fin and tube heat exchanger, where there is a lack of contact between the tube and the fin at the half of the tube's circumference. The aim of the present study is to numerically investigate the effect of the lack of contact on the energy efficiency of the heat exchanger for variable parameters, such as different air velocities and various position of the gap relative to the flow direction.

2 The scope of the study

The heat exchanger under consideration works as a condenser in a refrigeration system. It is a plate-fin and tube heat exchanger, in which the tubes

are arranged in-line. It was recognized that the location of the gap relative to the flow direction is an important parameter because of the variation in the local heat transfer coefficients on the surface of the fin and the locally variable velocity field [9]. The gap location along tube-fin joint circumference should therefore have a significant impact on heat exchange and flow patterns.

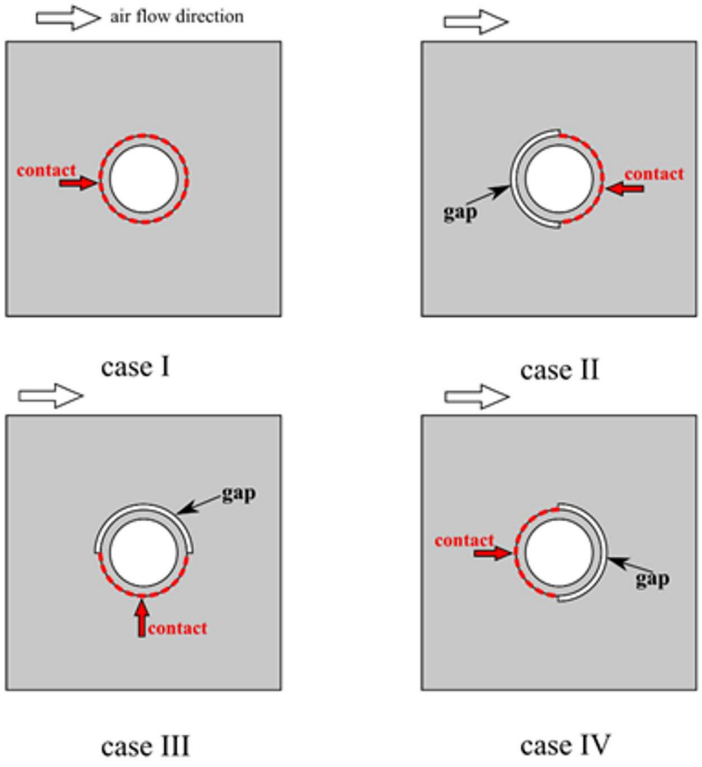

Figure 1: Different positions of the gap with respect to airflow: case I – without gap, case II – gap in the front of the tube, case III – gap in the top position, case IV – gap in the back of the tube.

Figure 1 shows the analyzed configurations. Case I (without a gap) is treated as a reference. In the second case, the gap spans the front side of the circumference. In the case III it is placed on the upper half perimeter, in the last, IV variant – in the back of the tube. Formation of the gap can be a result of non-ideal joint formation process or assembly requirements. For the egg-crate type heat exchangers, which are used as evaporators in

domestic refrigerators, slits between tubes are introduced to allow pulling the tube coil through the plate-fin packet [10]. In this case the lack of the contact is always present at approximately 1/2 perimeter of the tube and it is a feature essential for the assembly of the heat exchanger (geometry of this type of heat exchanger is shown in Fig. 2).

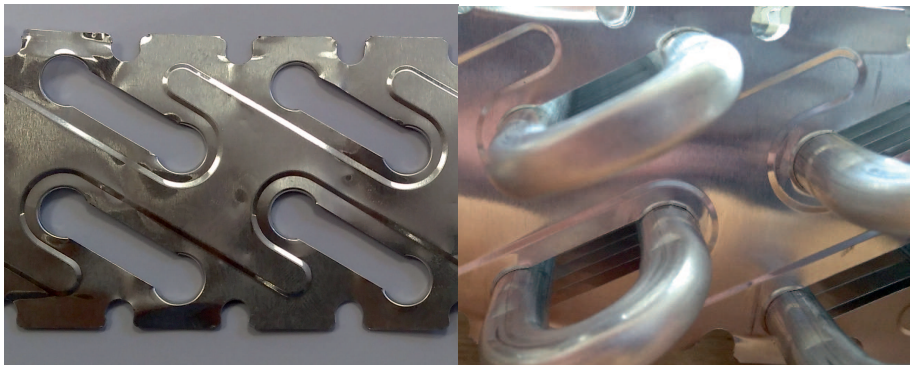

Figure 2: Geometry of egg-crate type heat exchanger: plate fin on the left, plate fin tube assembly on the right.

3 Numerical model of the heat exchanger

3.1 Geometry of the computational domain

The computational domain is a repeatable slice of the heat exchanger geometry, which is shown in Fig. 3. Length and width of the domain (L_f) are equal to the distance between the tubes axes. The thickness of the fin (δ_f) is a half of the actual fin thickness. Tube length in the domain equals to half of the distance between fins. Taking the half of inter-fin spacing is a consequence of the assumption flow symmetry. The specific values of the domain are given in Tab. 1.

3.2 Modeling of fluid flow with heat transfer

The SST (shear stress transport) turbulence model was chosen to solve Reynolds (time) averaged Navier-Stokes equations. SST combines the best features of k-ε and k-ω models. In the near wall region, approximately up to the half of boundary layer k-ω formulation is used, that does not require any damping functions. While for the outer zone of boundary layer k-ε is

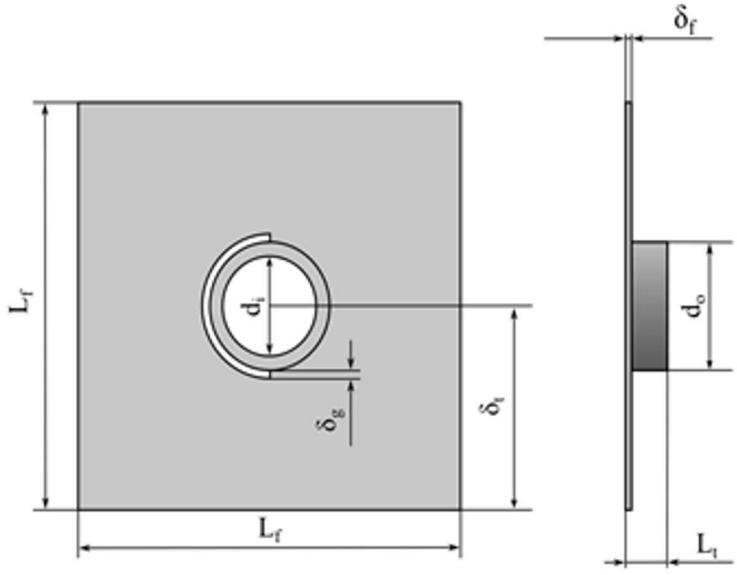

Figure 3: The geometry of the simulated slice of the heat exchanger.

the governing turbulence model – it eliminates the problem of k-ω sensitivity to values of ω in the freestream (outside the boundary layer). The other advantage of SST is the accurate prediction of the boundary layer separation by application of the turbulence production limiter in stagnation regions [11]. The SST model is also characterized by a very good accuracy of the numerical solutions for wall-bounded, complicated geometry flows, obtained with relatively low computational power. It is utilized in a number of works, where CFD analysis of heat transfer for finned and enhanced surfaces were carried out [6,12–16].

The following simplifying assumptions were made in the present work:

- steady state fluid flow and heat transfer,
- fluid flow and heat transfer are not periodic, the present study is valid for only the first row of heat exchanger,
- thermophysical properties of air are temperature dependent (ideal gas),
- mechanism of natural convection is considered negligible because the highest Richardson number calculated for simulation conditions is less than 0.1: $\mathrm{Ri}_{max} = (g\beta\Delta TL)/u^2 = 0.025$, where ΔT is is the temperature difference between fluid at heated surface and environment, g

is the gravitational acceleration, u and L are the characteristic length and velocity, respectively.

Numerical calculations were carried out using the commercial Ansys Fluent code capable of solving the Navier-Stokes equations [17].

Table 1: The dimensions of the domain for case II.

Description	Symbol	Value	Unit
Length and width of the fin	L_f	25.0	mm
Tube length	L_t	2.5	mm
Outside diameter of the tube	d_o	8.0	mm
Internal diameter of the tube	d_i	6.2	mm
Fin thickness	δ_f	0.1	mm
Gap width	δ_g	0.5	mm
Tube spacing	δ_t	12.5	mm

3.3 Boundary conditions

The computational domain is divided into three parts: air (fluid), fin and tube (solids). It was assumed that the thermal conductivity of the solid (aluminum) is constant for the tested temperature range, which is $\lambda = 202.4$ W/(m K). At the inlet to the domain (Fig. 4) uniform velocity and temperature profile were assumed:

$$T = T_{in}, \quad u_x = u_{in}, \; u_y = 0, \; u_z = 0, \tag{1}$$

where u_x, u_y, u_z are velocity components in x, y, z directions – according to coordinates system shown in Fig. 4. Values of k and ω at the inlet are determined by given, two parameters: turbulence intensity $I = 5\%$ and viscosity ratio $\mu_t/\mu = 10$:

$$k = \frac{3}{2}\left(u\, I\right)^2, \tag{2}$$

$$\omega = \rho \frac{k}{\mu} \left(\frac{\mu_t}{\mu}\right)^{-1}, \tag{3}$$

where μ_t is the turbulent viscosity. All boundary conditions values are given in Tab. 2. On the other surfaces of the computational domain symmetry

boundary condition was assigned, which can be expressed mathematically as

$$-\bar{n} \cdot \bar{\dot{q}} = 0, \quad \bar{u} \cdot \bar{n} = 0, \quad \nabla k \cdot \bar{n} = 0, \quad \nabla \omega \cdot \bar{n} = 0 \,, \tag{4}$$

where $\bar{n}$ is a normal vector to the surface on which the boundary condition was set $\bar{u}$ is the vector of velocity, and k, ω are the kinetic energy of turbulence and turbulence dissipation rate, respectively. Additionally, on the solid-fluid contact surfaces coupled type boundary condition was present, ensuring energy balance is satisfied between domains.

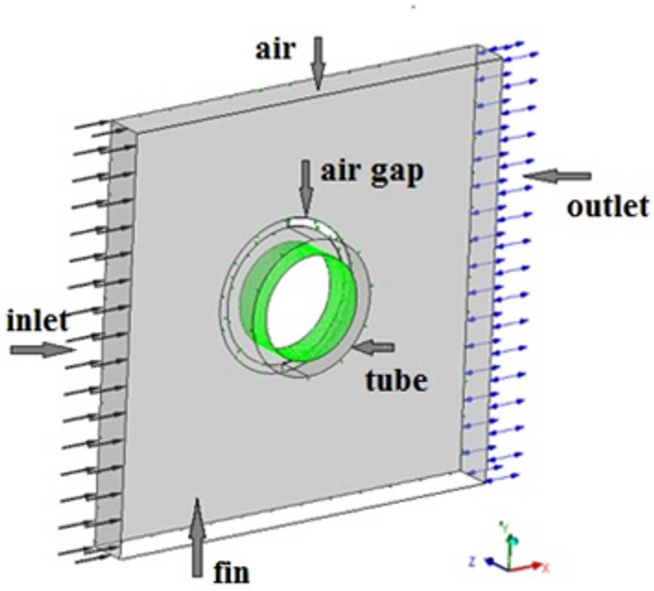

Figure 4: Computational domain with the boundary conditions.

3.4 Validation of the numerical simulations

The simulation results were validated by comparison with data available in open literature traditionally reported as j (Colburn factor) and f (friction factor) *vs.* Re_{do} defined as:

$$j = \frac{\bar{\alpha}}{\rho \, u_{\max} \, c_p} \, \mathrm{Pr}^{2/3} \,, \tag{5}$$

$$f = \frac{2 A_{\min} \, \Delta p}{A_{tot} \, \rho \, u_{\max}^2} \,, \tag{6}$$

Table 2: The values of quantities defining the boundary conditions.

Description	Symbol	Value	Unit
Temperature at inner surface of the tube wall	T_w	40	°C
Inlet air temperature	T_{in}	22	°C
Inlet air velocity	u_{in}	1–5	m/s
Gauge pressure at the outlet	p_{out}	0.0	Pa
Outlet air temperature	T_{out}	30	°C
Turbulence intensity at inlet/outlet	I	5	%
Viscosity ratio	μ_t/μ	10	–

$$\mathrm{Re}_{do} = \frac{u_{\max}\,\rho\,d_o}{\mu}\,, \tag{7}$$

where: $\bar{\alpha}$ – average heat transfer coefficient, $u_{max} = u_{in}/\sigma$, Δp – static pressure drop occurring through core of heat exchanger. The term σ is the ratio of the minimum flow area to frontal (inlet) area. A_{min} and A_{tot} are minimum flow area and total heat transfer area, respectively. Every thermophysical property like air density (ρ), specific heat capacity (c_p) or Prandtl number (Pr) are evaluated as averages of inlet and outlet values.

Widely accepted correlation of Wang *et al.* [18] is used for reference. Wang *et al.* added their own experimental data to correlation database to extend its validity range (data for small tubes diameters) [19]. The span of the correlation usage is shown in Tab. 3. Comparing with dimensions given in Tab. 2 the examined heat exchanger geometry is within the correlation range.

Table 3: Range of the validity of Wang *et al.* [18] correlation.

N – number of rows	d_o, mm	F_p – fin pitch, mm	P_t – transverse tube pitch, mm	P_l – longitudinal tube pitch, mm	Re_{do}, –
1–6	6.35–12.7	1.19–8.7	17.7–31.75	12.4–27.5	200–10000

We use the recommended correlation for Colburn coefficient for *N=1* (one-row heat exchanger) [18]. As stated in [18] mean deviation between correlation and data points is 7.51% for Colburn factor and 8.31% for friction

factor. The uncertainties of the experimental data are ranging from 3.2% to 15.9% for the j factor and 3.3% to 22.3% for f [19]. The highest uncertainties were associated with the lowest Reynolds numbers. Taking into account the mean deviation and assuming linear change of uncertainties, expected range of results can be estimated for j: 23.7% – 0.0012960 Re_{do} % and for f: 31.0% – 0.0019388 Re_{do} %.

The Colburn factors from simulations were calculated according to Eq. (5), average heat transfer coefficients were obtained directly from:

$$\bar{\alpha} = \frac{\dot{Q}}{A_{tot}\,\Delta T_{\log}}\,, \tag{8}$$

where

$$\Delta T_{\log} = \frac{T_{out} - T_{in}}{\ln\left(\frac{T_w - T_{in}}{T_w - T_{out}}\right)}\,, \tag{9}$$

and $\dot{Q}$ is the net heat transfer rate from numerical simulation, and T_w denotes average wall (fin) temperature from the simulation.

Alternatively $\bar{\alpha}$ were calculated using the reduction method as in [19] based on ε-NTU. This way one obtains UA and average air side heat transfer coefficient can be obtained from overall heat transfer resistance:

$$\frac{1}{U\,A} = \frac{\ln\left(\frac{d_o}{d_i}\right)}{2\,\pi\,L_t\,\lambda_w} + \frac{1}{\bar{\alpha}\;(A_t + \eta\,A_f)}\,, \tag{10}$$

where η is the fin efficiency. The method for obtaining the fin efficiency is the same as in Wang *et al.* [19] where Schmidt [20] approach was applied to derive the following relationship:

$$\frac{R_{eq}}{r} = 1.27\,\left(\frac{P_t}{d_o}\right)\,\sqrt{\frac{P_l}{P_t} - 0.3}\,. \tag{11}$$

where P_t is the transverse tube pitch, and P_l is the longitudinal tube pitch. This equation was the only formula cited in [19] for equivalent fin radius (R_{eq}), yet it is valid only for multi-row staggered tube layout. For the considered in present work one-row layout slightly different correlation should be used [20]:

$$\frac{R_{eq}}{r} = 1.28\,\left(\frac{P_t}{d_o}\right)\,\sqrt{\frac{P_l}{P_t} - 0.2}\,. \tag{12}$$

Because the overall heat transfer resistance – Eq. (10) depends on $\bar{\alpha}$ and on

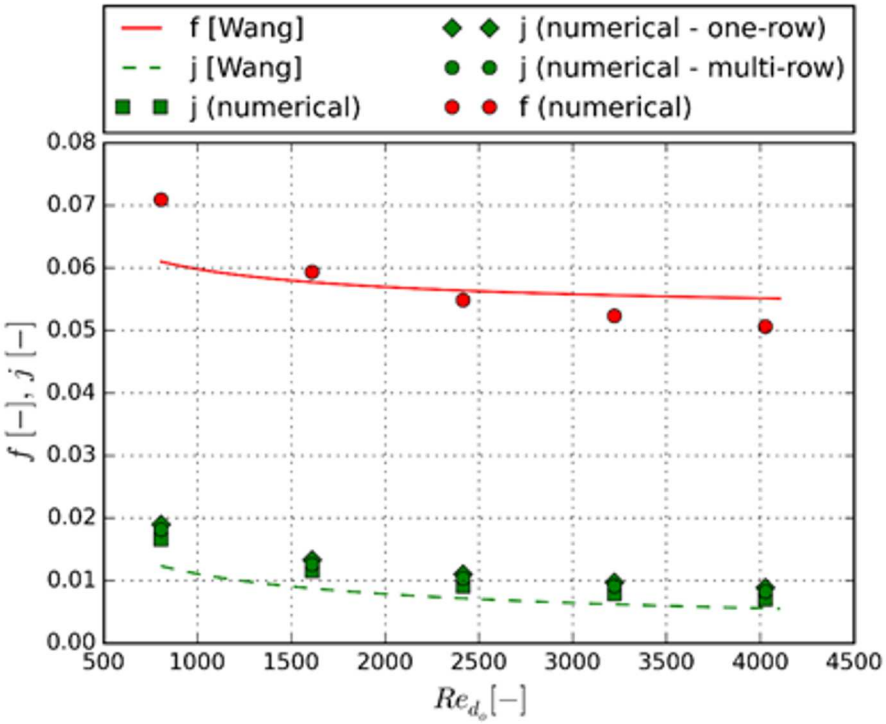

Figure 5: Comparison of Colburn and friction factors obtained from numerical simulation and from Wang *et al.* [18] correlation.

η which also is dependent on average heat transfer coefficient, the iteration procedure is used to solve for $\bar{\alpha}$. The friction factor is obtained from (6), where ΔP is a total pressure drop between the inlet and the outlet of the numerical domain. The comparison between numerical and experimental j and f factors (from Wang *et al.* correlation [18]) is shown in Fig. 5. The correlation values (continuous lines) and numerical ones (markers) are presented. Simulation results reflect approximately the trends of the j and f factors correlations. Although numerical friction factors are characterized by very good agreement with Wang *et al.* formula [18], CFD simulations considerably overpredict Colburn factors. This is more explicitly showed in Fig. 6 where the percentage differences between correlation and numerical values are plotted. In both of the plots three sets of numerical data are presented for j factor. They differ by the reduction methods – the first (numerical one) relies directly on numerical results. The second and

third are based on the reduction procedure applied in [19]. In numerical – 'one-row' data series – Eq. (12) is used for calculation of an equivalent fin radius, whereas in numerical – 'multi-row' Eq. (11) is utilized. The 'one-row' method is the most divergent from the correlation (relative difference from 50% to nearly 60%), the multi-row is similar but 5–10% lower on average. Direct calculation from Eq. (8) is the closest one to the correlation (approx. 30% to 35%).

This outcome is unexpected because in the Wang *et al.* [19] Schmidt [20] formula was used to obtain fin efficiency, so to get the best agreement with the correlation, one should utilize Schmidt equation to calculate η. Usage of the same reduction procedure as in the experiment should result with better convergence, although the effect is the opposite. This is caused by on the average 20% lower efficiencies calculated from Schmidt [20] than retrieved directly from numerical simulations.

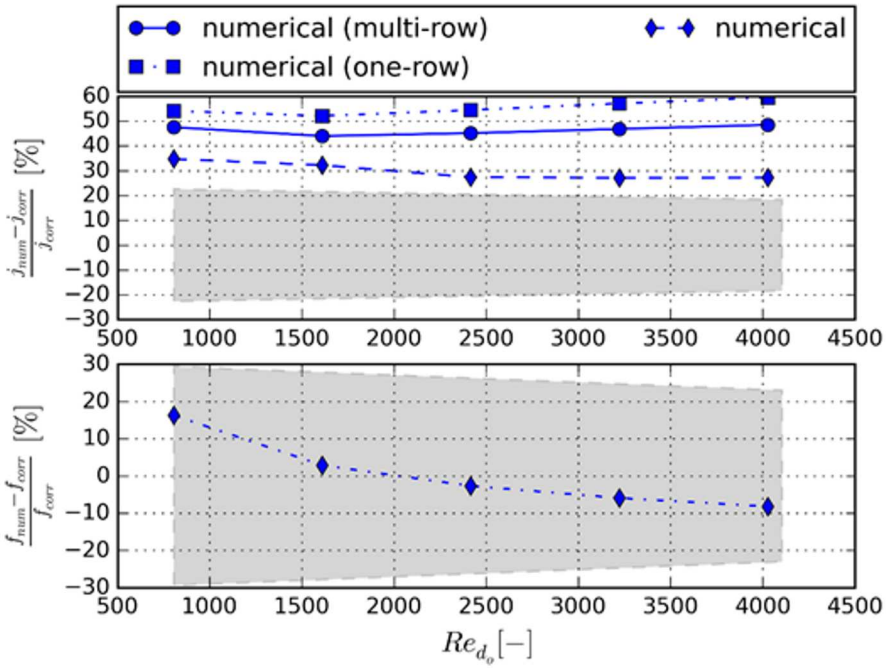

Figure 6: Relative differences between numerical and values calculated from correlation [18] of Colburn and friction factors in the function of Reynolds number.

Figure 6 depicts also relative differences of friction factors which are within uncertainty plus correlation scatter band (grey area). For considered Rey-

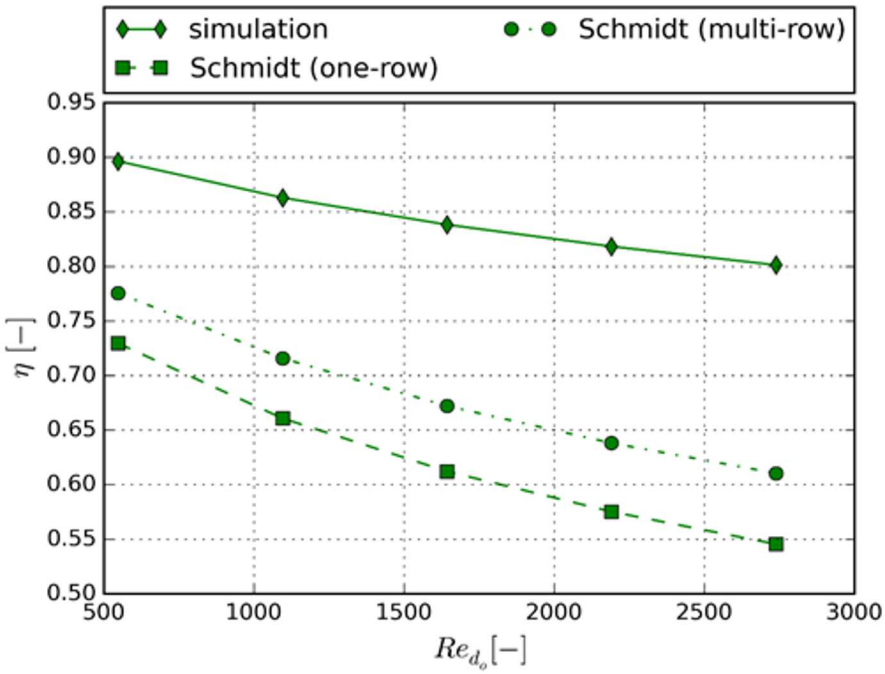

Figure 7: Fin efficiency in the function of Reynolds number, obtained directly from simulation, and by Schmidt [20] formula for one-row and multi-row tube arrangements.

nolds numbers range, there is practically −10–20% agreement with Wang *et al.* [18] formula. It is interesting that numerical friction factors are characterized by very good accordance, yet the j-Colburn factors are clearly above the expected values range (from 10% to 15% higher). This overprediction can be explained by some heat transfer enhancement caused by turbulence (while flow could be purely laminar) and some possible geometrical differences between real and simplified heat exchanger geometry applied in numerical simulations. Also the examined geometry could indicate bigger difference between fitted experimental data and the correlation than mean deviation (94% of experimental data were correlated with ±20% accuracy). In Fig. 8 relative differences between Colburn factors obtained from turbulent and laminar simulations is presented. Clearly flow turbulence augments heat transfer significantly even for lowest velocities (6% for lowest Reynolds number to 16% for highest one). The turbulence level is dependent on fin pitch, as small distance between fins damps the turbulence

development. In the examined case fin pitch is relatively big, therefore the turbulence should be present at least for the highest velocities. If the j-factors were lowered, assuming pure laminar flow, the part of the numerical data would be inside expected values range (for 'numerical' dataset).

To summarize, the friction factors retrieved from numerical simulations are in a good agreement with Wang *et al.* correlation [18]. The Colburn factors are overpredicted, yet some possible explanations were given for this situation. The trends of numerical results match trends of the data calculated from the validation formulas [18] with good accuracy. Overall accordance with the correlation is considered as sufficient to predict the flow and heat transfer for one-row tube arrangement.

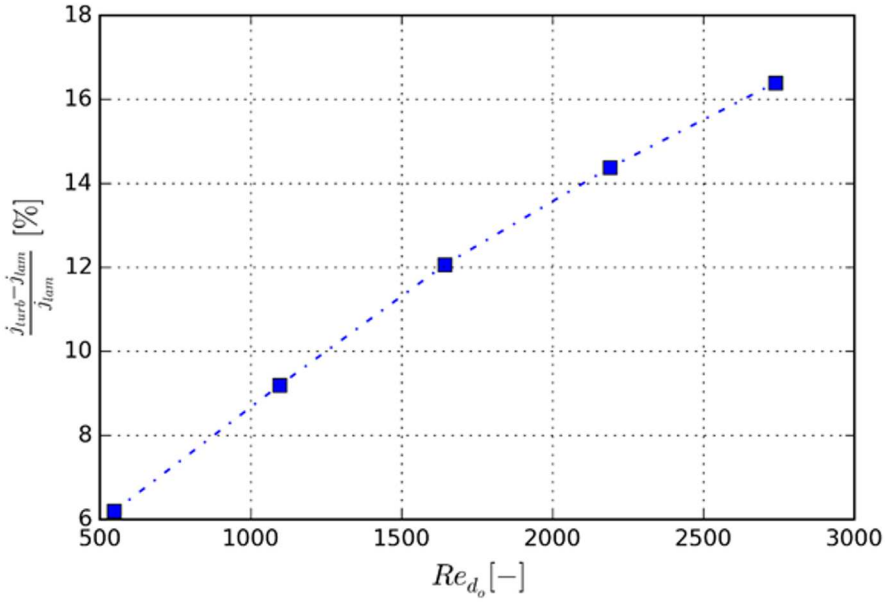

Figure 8: Relative difference between j-factors obtained from turbulent and laminar simulations.

4 Results and discussion

For each of the simulated cases the temperature field on the surface of the fin and structure of flow over the finned geometry were examined. For the reliable comparison of the variants with different average velocity the

dimensionless temperature excess is introduced

$$\theta = \frac{T_f - T_{in}}{T_w - T_{in}} \,. \tag{13}$$

The excess values can vary in the range from $\theta = 1$ if the fin temperature equals to the temperature of its root, up to $\theta = 0$ if fin cools to the inlet temperature of the air. In Fig. 9 distribution of the dimensionless excess temperature on the surface of the fin is presented for four considered gap positions and an example 5 m/s average velocity of the air. For other velocities dimensionless temperature excess distribution on the fin surface is analogous.

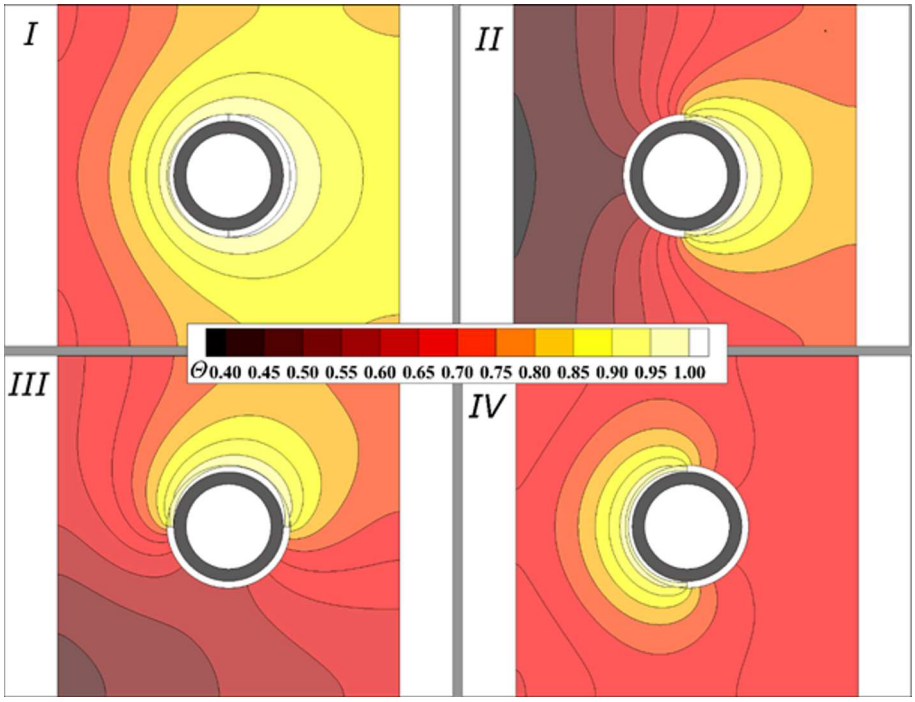

Figure 9: Distribution of θ on the surface of the fin at average inlet velocity $u = 5$ m/s for 4 analyzed cases.

For the variant without the gap the highest average temperature of fin was obtained, in opposition to case II, where the lowest temperatures are noted (on the front edge of the fin) – the gap in the front of the tube significantly reduces conducted heat flux to the frontal part of the fin.

Lack of the contact at the top position causes asymmetrical temperature and velocity distributions. Values of θ are significantly lower at the side where the gap is present, however mean fin temperature decreases less than in the case II. In the variant IV dimensionless temperature excess is lower for the fin region in the back of the tube, although it increases in the front area. Case IV seems to be the closest to the variant with ideal contact between the fin and the tube. Briefly summarizing the fluid flow in the domain: its structure changes the most significantly for the top position of the gap, yet the disturbance of the flow by the presence of the gap is generally very small. The air stream flowing through the channel of the heat exchanger flows around a tube and divides into two jets, while recirculation zone with small air velocities forms in the middle region of the fin (wake effect). Figure 10 shows a distribution of a local heat transfer coefficient on the surface of the fin at average inlet velocity $u = 5$ m/s for 4 analyzed cases.

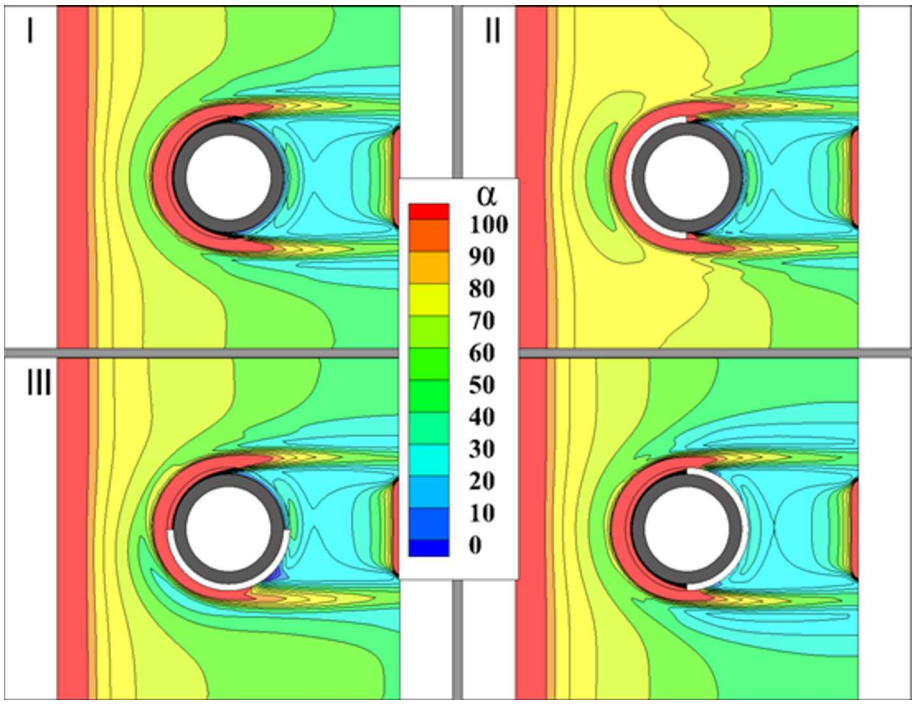

Figure 10: Distribution of α on the surface of the fin at average inlet velocity $u = 5$ m/s for 4 analyzed cases.

Local heat transfer coefficient α can be calculated using the equation:

$$\alpha = \left| \frac{\dot{q}}{(T_f - T_{in})} \right|, \tag{14}$$

where $\dot{q}$ is the local heat flux.

For all of the cases, highest values of α are seen in the region adjacent to the frontal (inlet) fin edge. It is an expected effect caused by the thermal boundary layer growth – boundary layer is the thinnest on the inlet fin edge. Behind the tube, in the recirculation zone, where the air velocity is the lowest the local heat transfer coefficient values are the lowest. In the front part of the fins, in the vicinity of the tubes, a band of intensified heat transfer is present, encircling the front half of the tube circumference. For the shown inlet velocity (5 m/s) a horseshoe shape of the high α band is clearly visible. As fluid velocity increases from the initial 1 m/s value, width and length of the band also increases, and it adapts to a horseshoe shape. This local heat transfer intensification is caused by the presence of the horseshoe vortex in the front of the tube (described in detail in [9]). For the case II and III interesting effect of the gap presence can be seen. The gap positioned in the front of the tube limits the area spanned by the wake behind the tube. This effect is the most evident in the III case, in which at the top side of the fin distribution of α is the same as for variant I, however at the gap side area of the low α region decreases. The reduction of the recirculation region is the greatest for the case II, although the loss of heat transfer surface in the front of the tube decreases heat transfer enhancement due to horseshoe vortex and blocks heat flow toward front region of the fin, where highest heat transfer coefficients are noted. As a result the positive effect of the narrowing the wake is diminished by the above mentioned phenomena.

Localization of the gap behind the tube, results in the widest region of low heat transfer intensity. However there is the difference in the distributions α at top and bottom halves of the fin. For example in the case II, there is the biggest zone with α in the range of 60–80 W/(m K) ranging almost up to the back edge of the fin. This zone is the smallest for the variant IV while for I and III it spans only front half of the fin (although in the case III asymmetry of the flow seems to decrease the zone). The front position of the gap elongates the intensification gap, due the influence of the horseshoe vortex, what can be seen best in the case III, where the 'arms' of the horseshoe structure have different lengths (longer on the gap side).

Absolute measure of thermal efficiency of the considered slice of the heat exchanger can be expressed as the total exchanged heat transfer rate. It is related to heat transfer rate for the case I (without the gap). In Fig. 11 the ratio of the heat transfer rate for given case to the heat transfer rate for case I versus average inlet air velocity is plotted.

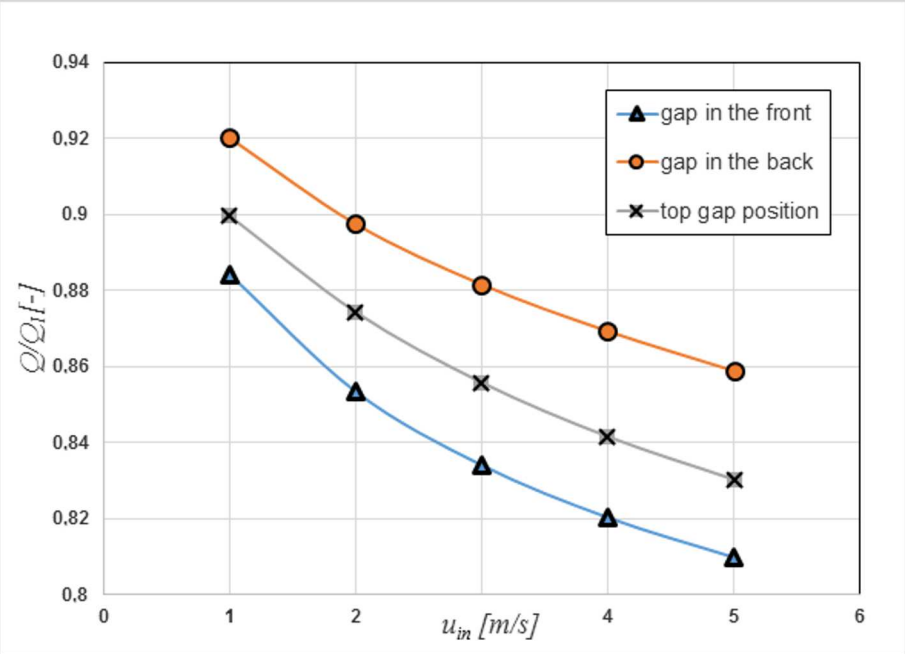

Figure 11: Ratio of the heat transfer rate for given case to the heat transfer rate for case I versus average inlet air velocity.

Variant with the gap in the back of the tube turned out to be the most similar to the full contact. It is characterized by only 8% heat transfer rate decrease relative to the case I. As the velocity increases relative difference increases to 14% for maximum considered velocity. All of the variants are characterized by a similar trend. The top position of the gap (case III) is less efficient than the case IV – for the velocity 1 m/s it reaches 90% of thermal throughput of the ideal contact, although for 5 m/s it decreases to 83%. Frontal localization the gap reduces heat transfer rate the most – relatively by 12% for 1 m/s and by 19% for 5 m/s. Intensification of heat transfer, mentioned earlier caused by the reduction of the recirculation zone for the case II is compensated fully by the negative lack of contact effect. It shows that the lack of contact on the given part of the circumference

has the key importance. The gap in the front blocks the heat flow to the fin region where heat transfer intensity is the greatest. Top localization blocks only a half of the frontal circumference, and a second half where heat is conducted towards rear region characterized by the lowest local heat transfer coefficients. The lack of contact behind the tube decreases thermal efficiency less, because of the wake forming behind the tube, parallel to the heat flow. The distributions of the heat transfer coefficient on the surface of the fin for individual cases allow to conclude, that the heat transfer intensification by cutting the gaps in the frontal area of the fin, in the vicinity of the tube, is possible. Negative influence of a lack of the contact can be reduced by the application of smaller, shorter gaps that are positioned further from the base of the fin. Analysis of heat transfer intensification caused by the cutting of such gaps on the surface of the fin is an attractive direction of the future research.

5 Conclusions and summary

Numerical study of heat transfer and fluid flow of the first row of the plate-fin and tube heat exchanger were carried out, analyzing influence of the lack of contact between fin and tube for the various gap localizations relative to the flow direction (case I – full contact, II – gap in the front of the tube, III – top position, IV – gap in the back of the tube). The computational fluid dynamics analysis was made for the range of average air velocities: 1–5 m/s. Key findings of the study are given in the points below:

- the lack of contact between a tube and a fin influences significantly the fin temperature distribution,
- the lowest average fin temperature was obtained for the gap in the front, the highest for the gap in the back,
- in the case II (frontal gap) there is some heat transfer intensification present due to reduction of the wake area behind the tube,
- the highest net heat transfer rate is exchanged for the case where the gap was located in the back (average decrease by 8% for 1 m/s relatively to the full contact case) and the least for the gap in the front position (12% decrease for 1 m/s), for the top gap position – 10%,

- potentially, there is a possibility to intensify heat transfer by the positioning of the gaps, in the vicinity of the tube – in some distance from the fin base.

Received 16 December 2017

References

[1] Tang Ding, Li Dayong, Peng Yinghong: *Optimization to the tube–fin contact status of the tube expansion process*. J. Mater. Process. Tech. **211**(2011), 4, 573–577.

[2] Critoph R.E., Holland M.K., Turner L.: *Contact resistance in air-cooled plate fin-tube air-conditioning condensers*. Int. J. Refrig. **19**(1996), 6, 400–406.

[3] Jannick P., Meurer C., Swidersky H.W.: *Potential of Brazed Finned Tube Heat Exchangers in Comparison to Mechanical Produced Finned Tube Heat Exchangers*. In: Proc. Int. Refrigeration and Air Conditioning Conf., Purdue University, 2002.

[4] Jeong Jin, Nyung Kim Chang, Youn Baek, Saeng Kim Young: *A study on the correlation between the thermal contact conductance and effective factors in fin–tube heat exchangers with 9.52 mm tube*. Int. J. Heat. Fluid Fl. **25**(2004), 6, 1006–1014.

[5] Cheng Wui-wai, Madhusudana Chakravarti: *Effect of electroplating on the thermal conductance of fin–tube interface*. Appl. Therm. Eng. **26**(2006), 17–18, 2119–2131.

[6] Taler D., Ocłoń P.: *Thermal contact resistance in plate fin-and-tube heat exchangers, determined by experimental data and CFD simulations*. Int. J. Therm. Sci. **84**(2014), 309–322.

[7] Taler D., Cebula A.: *A new method for determination of thermal contact resistance of a fin-to-tube attachment in plate fin-and-tube heat exchangers*. Inżynieria Chemiczna i Procesowa **31**(2010), 4, 839–855.

[8] Singh Shobhana, Sørensen Kim, Condra Thomas J.: *Influence of the degree of thermal contact in fin and tube heat exchanger: A numerical analysis*. Appl. Therm. Eng. **107**(2016), 612–624.

[9] Bansal P.K., Wich T., Browne M.W.: *Optimisation of egg-crate type evaporators in domestic refrigerators*. Appl. Therm. Eng. **21**(2001), 7, 751–770.

[10] Rosman E.C., Carajilescov P.P., Saboya F.M.: *Performance of one- and two-row tube and plate fin heat exchangers*. ASME. J. Heat Transfer, **106**(1984), 3, 627–632.

[11] Menter F.R.: *Zonal two equation kappa-omega turbulence models for aerodynamic flows*. In: Proc. 24th Fluid Dynamics Conf., Orlando, Florida, 6-9 July 1993.

[12] Taler D., Ocłoń P.: *Determination of heat transfer formulas for gas flow in fin-and-tube heat exchanger with oval tubes using CFD simulations*. Chem. Eng. Process.: Process Intensification **83**(2014), 1–11.

[13] Babak Lotfi, Min Zeng, Bengt Sundén, Qiuwang Wang: *3D numerical investigation of flow and heat transfer characteristics in smooth wavy fin-and-elliptical tube heat exchangers using new type vortex generators*. Energy **73**(2014), 233–257.

[14] Jasiński P.B.: *Numerical study of thermo-hydraulic characteristics in a circular tube with ball turbulators. Part 3: Thermal performance analysis*. Int. J. Heat.Mass Tran. **107**(2017), 1138–1147.

[15] Ansys Inc., *ANSYS Fluent Theory Guide*. 2013.

[16] Muszyński T., Kozieł S. M.: *Fluid flow consideration in fin-tube heat exchanger optimization*. Arch. Thermodyn. **37**(2010), 3, 45–62.

[17] Wais Piotr: *Fluid flow consideration in fin-tube heat exchanger optimization*. Arch. Thermodyn. **31**(2010), 3, 87–104.

[18] Wang Chi-Chuan, Chi Kuan-Yu, Chan Chun-Jung: *Heat transfer and friction characteristics of plain fin-and-tube heat exchangers. Part II: Correlation*. Int. J. Heat Mass Tran. **43**(2000), 2693–2700.

[19] Wang Chi-Chuan, Chi Kuan-Yu: *Heat transfer and friction characteristics of plain fin-and-tube heat exchangers. Part I: New experimental data*. Int. J. Heat Mass Tran. **43**(2000), 2681–2691.

[20] Schmidt Th.E.: *Heat transfer calculations for extended surfaces*. Refrig. Eng. **57**(1949), 351–357.